Biosensors and Bioelectronics 203 (2022) 114011

Contents lists available at ScienceDirect

Biosensors and Bioelectronics

journal homepage: www.elsevier.com/locate/bios

Effects of defective motors on the active transport in biosensors powered by biomolecular motors

Samuel Macharia Kang'iri [a], Andrew Salem [b], Dan V. Nicolau [b,**], Takahiro Nitta [a,*]

[a] Faculty of Engineering, Gifu University, Gifu, 501-1193, Japan
[b] Department of Bioengineering, Faculty of Engineering, McGill University, Montreal, Quebec, H3A 0C3, Canada

ARTICLE INFO

Keywords:
Active transport
Motor protein
Brownian dynamics simulation
Polymer surface

ABSTRACT

Motor proteins, such as myosin and kinesin, are biological molecular motors involved in force generation and intracellular transport in living cells. They were proposed to drive molecular shuttles for the active transport of analytes, thus significantly accelerating the sensing process of biosensors. Integrating motor proteins into biosensors requires their immobilisation on the operating surfaces. However, this process makes some motor proteins defective, slowing analyte detection. Here, we investigated the movements of molecular shuttles on surfaces in the presence of active and defective motors using a Brownian dynamics simulation, and elucidated the effects of defective motor proteins on the transport efficiency of the shuttles. We found that the motility of shuttles depends on the fraction of active motors relative to defective ones and that over 90% of the surface-bound motor proteins must remain active for efficient transport. The high fraction of active motors required for efficient transport can be attributed to the difference in the binding lifetimes of active and defective motors to shuttles. These results provide insights into how motors accumulate on sensor surfaces and set a guideline for the choice of polymer materials for biosensors powered by motor proteins.

1. Introduction

Motor proteins, such as those in the myosin and kinesin families with typical sizes of several tens of nanometres, are biological molecular motors involved in force generation and intracellular transport in living cells (Vale and Milligan, 2000). Because they convert chemical energy stored in adenosine triphosphate (ATP) into kinetic energy with high efficiency and are inherently compatible with other biomolecules, motor proteins are interesting dynamic nanomachines that do not require external devices such as pumps (Agarwal and Hess, 2010; Bachand et al., 2009, 2014; Bakewell and Nicolau, 2007; Goel and Vogel, 2008; Korten et al., 2010; Månsson, 2012; Saper and Hess, 2020). Among the devices proposed to use motor proteins, biosensors are arguably the most promising (Fischer et al., 2009; Lard et al., 2013; Lin et al., 2008), as the active transport of analytes by motor proteins could overcome the mass transport limitation (Katira and Hess, 2010; Nitta and Hess, 2013; Sheehan and Whitman, 2005; Soleymani and Li, 2017), which is a significant bottleneck in conventional biosensors.

A typical implementation of biosensors powered by motor proteins consists of analyte-loading molecular shuttles propelled by motor proteins (Hess, 2011; Korten et al., 2010), moving along predefined tracks toward a detection area (Hess et al., 2001; Hiratsuka et al., 2001). A significant benefit of using myosin, or its proteolytic fragment, heavy meromyosin (HMM), is its higher transport speed than kinesin (Månsson, 2012; Reuther et al., 2021). Consequently, once the tracks for molecular shuttles are appropriately designed (Nitta et al., 2008; Sunagawa et al., 2013), the detection time of biosensors powered by the HMM is inherently significantly shorter (Nitta and Hess, 2013).

When the HMM is immobilised on the working surface of the biosensors, some of these proteins denature and cannot hydrolyse ATP. These defective HMM molecules, termed rigor heads, can bind to actin filaments. However, they cannot translate them, thus inhibiting the movement of actin filaments. Beyond a certain threshold, defective HMMs will lower the performance of biosensors powered by motor proteins (Lard et al., 2013), because of the lower gliding speed of actin filaments or outright halting of the movement. Despite the importance of surface-induced modulation of the bioactivity of motor proteins, experimental difficulties have hampered systematic investigations on the effects of defective HMMs. We adapted previously reported Brownian dynamics simulations (Ishigure and Nitta, 2014, 2015) and studied

* Corresponding author. Applied Physics Course, Faculty of Engineering, Gifu University, 1-1Yanagido, Gifu, 501-1193, Japan.
** Corresponding author. Department of Bioengineering, Faculty of Engineering, McGill University, Montreal, QC, H3A 0E9, Canada.
E-mail addresses: dan.nicolau@mcgill.ca (D.V. Nicolau), nittat@gifu-u.ac.jp (T. Nitta).

https://doi.org/10.1016/j.bios.2022.114011
Received 22 October 2021; Received in revised form 30 December 2021; Accepted 14 January 2022
Available online 19 January 2022

the effects of the defective HMMs on the transport efficiency of the shuttles and compared the simulation results with an experimental study reporting the total number of HMMs on various surfaces and the HMM bioactivity (Hanson et al., 2017). The advantage of using computer simulation is that it allows the precise control of the number of defective HMMs and provides information on which HMM binds to the actin filaments and generates force using well-established constitutive equations and parameters.

2. Methods

Fig. 1 schematically presents the simulation method used for reproducing the movement of actin filaments gliding over flat surfaces covered with active and defective HMMs. The actin filaments were modeled as inextensible semiflexible bead-rod polymers with a flexural rigidity of $EI = 0.073$ pN·μm^2 (Gittes et al., 1993). The default length of the filament was set to 3 μm. Because transport speed was our primary focus, no breakage of actin filaments was assumed. Active and defective HMMs were placed on substrates in the ratio ($r_{substrate}$):

$$r_{substrate} = \frac{[active\ HMM]}{[active\ HMM] + [defective\ HMM]} \quad (1)$$

The active and defective HMMs were modeled as linear springs which could bind to actin filaments. The active HMMs can undergo ATP hydrolysis cycles described with a four-state model (Walcott et al., 2012), thus propelling actin filaments. The defective HMMs remain bound to actin filaments until tension builds up and reaches the threshold of the detachment force of 9.2 pN (Nishizaka et al., 1995), thus impeding translocation of actin filaments. More detailed descriptions of the simulation method are provided in the Supplementary Information.

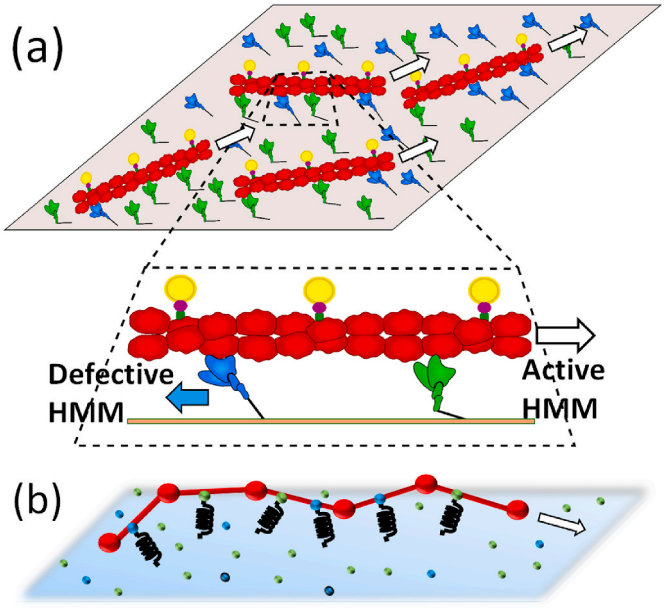

Fig. 1. (a) Schematic of molecular shuttles based on actin filaments gliding over a surface with active (green) and defective (blue) HMMs. The active HMMs (green) facilitate the forward movement, while the defective HMMs (blue) act as effective friction. (b) Schematic representation of the simulation method. An actin filament was represented as a bead-rod polymer. Active and defective HMMs were represented as linear springs. (For interpretation of the references to colour in this figure legend, the reader is referred to the Web version of this article.)

3. Results and discussion

3.1. Trajectories of actin filaments gliding over active and defective motors

The impact of defective HMMs on the gliding speed of actin filaments was investigated by simulating motility while systematically changing $r_{substrate}$. Fig. 2a shows the results of representative movements of actin filaments for a duration of 5 s on surfaces presenting various $r_{substrate}$. At low $r_{substrate}$, actin filaments had virtually no translation (Fig. 2a, $r_{substrate} = 0.70$). At a high $r_{substrate}$, the actin filaments moved continuously (Fig. 2a, $r_{substrate} = 0.98$). At a threshold of $r_{substrate}$ of 0.94, actin filaments showed undulating motions, similar to those observed experimentally (Bourdieu et al., 1995). Representative trajectories of the leading tips of actin filaments gliding over surfaces covered with active and defective HMMs are shown in Supplementary Information Fig. S1.

3.2. Gliding speeds of actin filaments over active and defective motors

To quantify the effects of defective HMMs, the gliding speed of actin filaments was recorded as a function of $r_{substrate}$ (Fig. 2b and Supplementary Information Fig. S2). The actin filaments were unable to move or glide very slowly until $r_{substrate}$ of approximately 0.9 was reached, showing that the denaturation of 10% of the HMMs immobilised on the working surfaces of the biosensors halted the transport. Above this threshold, the gliding speed of the actin filaments showed a linear increase. Interestingly, the gliding speed of actin filaments on HMM-functionalised surfaces was more sensitive to the concentration of defective HMMs than that presented by microtubules moving over kinesin-functionalised surfaces (Scharrel et al., 2014).

This analysis suggests that, while the biosensors integrated with the HMMs in their operation offer advantages regarding the speed of analyte detection, resilient sensitivity of the gliding speed of the molecular shuttles to the density of defective HMMs requires considerable attention. Indeed, for the HMM-based motility assays, the imperativeness for minimisation of the density of defective HMMs has been addressed: (i) at the pre-fabrication stage, e.g., using appropriate storing of motor proteins (Albet-Torres and Månsson, 2011); (ii) at the fabrication stage, i.e., via the selection of surfaces that maximise the adsorption of motor proteins, but also those that preserve their bioactivity (Hanson et al., 2017; Nicolau et al., 2007); (iii) at the pre-operation stage, e.g., via the blockage of the defective HMM by 'sacrificial' actin filaments (Rahman et al., 2018), a procedure not used for kinesin-based motility assays; and finally (iv) during operation, by avoiding or removing chemical species known to deactivate HMMs, e.g., reactive oxygen (Harada et al., 1990), or by altering the function of HMMs (Diensthuber et al., 2011); or conversely by using chemical species that 'reactivate' the HMMs (Diensthuber et al., 2011).

3.3. The number of binding motors

The mechanism of the onset of gliding movement was revealed by investigating the binding of active and defective HMMs. During the onset of gliding movements, the number of binding active and defective HMMs fluctuated around their average due to repeated binding to and detachment from the actin filaments (Supplementary Information Fig. S3). The time-averaged number of defective binding HMMs decreased monotonically with an increase in $r_{substrate}$. Whereas the time-averaged number of binding active HMMs remained high until around the value of $r_{substrate}$ that induced the onset of gliding movements of actin filaments, and it dropped at higher active HMM ratios (Fig. 2c).

To understand the differences in the population of HMMs binding to actin filaments, we defined the ratio of binding active HMMs as

$$r_{binding} = \frac{n_{binding,active}}{n_{binding,active} + n_{binding,defective}}, \quad (2)$$

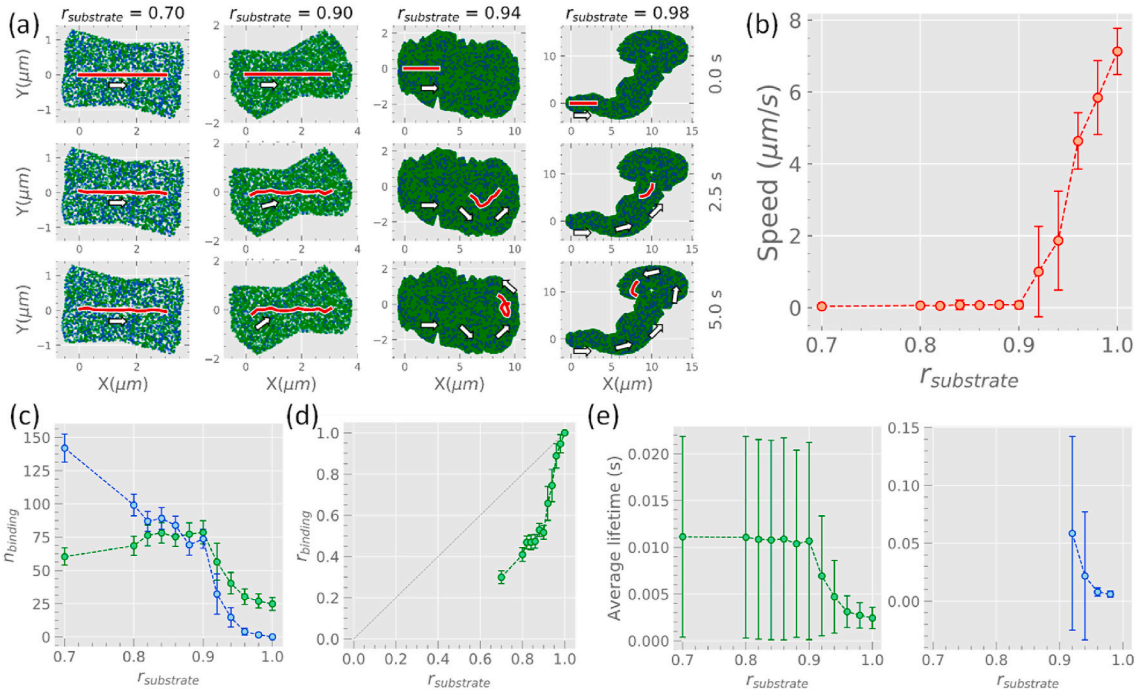

Fig. 2. Simulation results. (a) Snapshots of actin filaments on HMM-covered surfaces with various $r_{substrate}$. Green and blue dots represent active and defective HMMs, respectively. (b) The gliding speed of actin filaments on surfaces with various $r_{substrate}$. The HMM density was 3000 μm^{-2}. ATP concentration was 2000 μM. The length of the actin filament was 3 μm. (c) The average numbers of binding active (green) and defective (blue) HMMs as a function of $r_{substrate}$. (d) $r_{binding}$ as a function of $r_{substrate}$. (e) The average life binding lifetimes of active (left) and defective (right) HMMs. Below $r_{substrate}$ of 0.92, the binding lifetime of defective motor exceeded the simulated time of 5 s. Error bars represent standard deviations of the data in (b, c, d, e). The large error bars in (e) result from the distributions of lifetimes shown in Supplementary Information Fig. S4. (For interpretation of the references to colour in this figure legend, the reader is referred to the Web version of this article.)

where $n_{binding,active}$ and $n_{binding,defective}$ are the numbers of active and defective HMMs binding to actin filaments, respectively. $r_{binding}$ was found to be smaller than $r_{substrate}$ (Fig. 2d). For example, although 80% of the HMMs were active on substrates, only about 40% of binding HMMs propelled actin filaments. This discrepancy between $r_{substrate}$ and $r_{binding}$ indicates that high $r_{substrate}$ values are required to overcome the impedance generated by defective HMMs, which explains the particularly narrow range for the values of $r_{substrate}$ that supports the continuous movement of actin filaments. Based on this observation, a possible way to reduce the minimum value of $r_{substrate}$ required for the continuous movements of actin filaments is to reduce the detachment force of HMMs.

The discrepancy between $r_{binding}$ and $r_{substrate}$ was caused by a difference in the binding lifetimes of active and defective HMMs against $r_{substrate}$ (Fig. 2e). The binding lifetime of active HMMs remained relatively constant at approximately 0.011 s until $r_{substrate}$ was approximately 0.9, and then dropped to approximately 0.002 s. The prolonged binding lifetime at low $r_{substrate}$ was due to the slowing down of ADP release caused by the impedance from defective HMMs, as explained in the Supplementary Information, equation (S1). The decreasing number of binding active HMMs (Fig. 2c) resulted from the decrease in the binding lifetime (Fig. 2e, left), which dominated the increasing number of active HMMs on the substrate.

The binding lifetime of defective HMMs monotonically decreased with an increase in $r_{substrate}$, because of the increase in the gliding speed of actin filaments, as it took a shorter time for the defective HMMs to be stretched to F_{detach}/k, where the detachment occurred. The decrease in the number of defective binding HMMs with an increase in $r_{substrate}$ resulted from a combined effect of the decrease in the number of defective HMMs on substrates and the binding lifetime (Fig. 2e, right).

3.4. Surface density of HMMs on polymer substrates

While our simulation study showed that 90% of the HMMs must be active to support sustainable movements of actin filaments, an experimental study (Hanson et al., 2017), which measured the total and active number of HMMs on various *polymeric* surfaces, reported that 10–70% of the active HMMs were sufficient to sustain a continuous movement of actin filaments. This discrepancy is discussed here. Discrepancies in speed and number of HMM molecules are discussed in Supplementary Information.

In motility assay experiments with HMM immobilised on polymers, the adsorbing 'surface' has a complex structure in the depth direction (presented schematically in Fig. 3). Quartz crystal microbalance measurements showed that the *total* number of adsorbed HMM molecules ranged, depending on the properties of the adsorbing polymeric surface, between approximately 4300 to 12,000 μm^{-2} (Hanson et al., 2017). Accounting for the dimensions of a myosin head domain (16.5 × 6.5 × 4.5 nm) (Lodish et al., 2016) and HMM step size (5–10 nm), such high densities of adsorbed HMMs are possible only in the form of multiple layers on substrates, with some of them embedded into polymer layers (Fig. 3, right). On the one hand, the HMM molecules cannot reach the rigid, bottom polymeric surface, as an elastomeric layer shields this. On the other hand, the large uptake of water at the top of a moderately hydrophobic polymer, for example, nitrocellulose, of up to 90%, creates a penetrable gel sheet, thus allowing HMM molecules to 'dissolve' in this layer. However, it is also likely that HMMs experience frequent steric interactions with the brush-like polymeric chains in the gel layer. Finally, the HMM molecules which are free of the entanglement of the loose polymeric chains, as well as away from hydrophobic polymeric regions, will exhibit a higher active HMM ratio than that suggested by the quartz microbalance measurements, which account for *all* the HMM molecules regardless of their position in the polymeric multi-layered material.

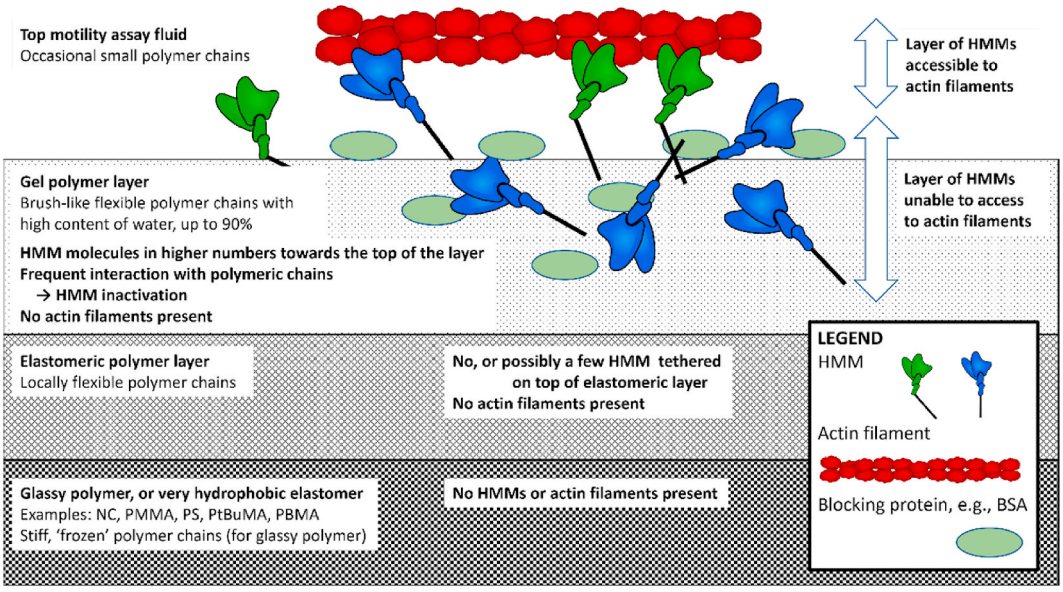

Fig. 3. Schematic illustration of the structuring of the adsorbing polymeric layer and the possible distribution of HMMs within the polymer layers.

Despite these complexities in the experiments, the simulation focused on the immobilised HMMs present in a single layer on the geometrically flat top surface (Fig. 3), accessible to actin filaments. Thus, the discrepancy between our simulation and the experiment can be explained by the HMM distribution into the depth of the polymer layers. For continuous transport, 90% of the HMMs in the top layer, and not in the whole layers, should be active.

Various surface-binding methods for kinesin motors via their engineered modification have been developed (Inoue et al., 2019) (Lam et al., 2018) (Romet-Lemonne et al., 2005) (Yu et al., 2005) and used for controlled immobilisation. However, because HMM-specific binding methods are rare, for example, the HMM-based antibodies (Winkelmann et al., 1995), surface binding of the HMMs relies in most cases on the non-specific adsorption of HMMs onto substrate materials. This is presumably because HMMs are usually extracted from muscle tissues. In contrast, kinesins are expressed in *Escherichia coli,* so engineered kinesins are relatively available.

These findings provide insight into the appropriate selection of the surfaces of biosensors employing HMMs for propelling actin filaments operating as molecular shuttles. Avoiding hydrophobic materials, which inherently induce the advanced denaturation of HMMs, is a necessary but insufficient condition for the effective operation of biosensors powered by HMMs (Nicolau et al., 2007). An additional and critical condition is the presence of a top gel polymeric layer, which gradually liberates HMMs from polymeric chain entanglements because of the large size and non-globular shape of HMM, thus securing the highly active HMM ratio at the interface with the buffer containing actin filaments. Examples of polymers that fulfill these requirements, i.e., reduced hydrophobicity and considerable water uptake in the top layer, are nitrocellulose, PMMA, and polystyrene, in that order (Hanson et al., 2017).

4. Conclusions

We investigated the effects of defective HMMs on the translocation of actin filaments, which act as molecular shuttles in biosensors powered by HMMs. We found that the motility of actin filaments was very sensitive to defective HMMs on the surface of biosensors. More specifically, more than 90% of surface-bound HMMs must remain active to achieve continuous transportation of actin filaments. We showed that this critical fraction for the onset of the gliding movement of actin filaments could be elucidated by the difference in binding lifetimes of active and defective HMMs. Given the values of the parameters of the mechanochemical cycle and the binding kinetics of HMMs, the fraction of active HMM was the critical factor determining whether actin filaments were motile. These findings provide fundamental insight into the appropriate selection of surface materials for biosensors employing HMMs for propelling actin filaments operating as molecular shuttles.

Declaration of competing interest

The authors declare that they have no known competing financial interests or personal relationships that could have appeared to influence the work reported in this paper.

Acknowledgments

This work was supported by grants from JSPS KAKENHI Grant Number 19H02106, the Natural Sciences and Engineering Research Council (NSERC) of Canada, Grant RGPIN-2016-05019, and the Social Sciences and Humanities Research Council of Canada (SSHRC), Grant NFRFE-2019-00129.

Appendix A. Supplementary data

Supplementary data to this article can be found online at https://doi.org/10.1016/j.bios.2022.114011.

References

Agarwal, A., Hess, H., 2010. Prog. Polym. Sci. 35, 252–277.
Albet-Torres, N., Månsson, A., 2011. Langmuir 27, 7108–7112.
Bachand, G.D., Bouxsein, N.F., VanDelinder, V., Bachand, M., 2014. Wiley Interdiscip. Rev. Nanomed. Nanobiotechnol. 6, 163–177.
Bachand, G.D., Hess, H., Ratna, B., Satir, P., Vogel, V., 2009. Lab Chip 9, 1661–1666.
Bakewell, D.J.G., Nicolau, D.V., 2007. Aust. J. Chem. 60, 314.
Bourdieu, L., Duke, T., Elowitz, M.B., Winkelmann, D.A., Leibler, S., Libchaber, A., 1995. Phys. Rev. Lett. 75, 176–179.
Diensthuber, R.P., Müller, M., Heissler, S.M., Taft, M.H., Chizhov, I., Manstein, D.J., 2011. FEBS Lett. 585, 767–771.
Fischer, T., Agarwal, A., Hess, H., 2009. Nat. Nanotechnol. 4, 162–166.
Gittes, F., Mickey, B., Nettleton, J., Howard, J., 1993. J. Cell Biol. 120, 923–934.
Goel, A., Vogel, V., 2008. Nat. Nanotechnol. 3, 465–475.
Hanson, K.L., Fulga, F., Dobroiu, S., Solana, G., Kaspar, O., Tokarova, V., Nicolau, D.V., 2017. Biosens. Bioelectron. 93, 305–314.
Harada, Y., Sakurada, K., Aoki, T., Thomas, D.D., Yanagida, T., 1990. J. Mol. Biol. 216, 49–68.
Hess, H., 2011. Annu. Rev. Biomed. Eng. 13, 429–450.

Hess, H., Clemmens, J., Qin, D., Howard, J., Vogel, V., 2001. Nano Lett. 1, 235–239.
Hiratsuka, Y., Tada, T., Oiwa, K., Kanayama, T., Uyeda, T.Q.P., 2001. Biophys. J. 81, 1555–1561.
Inoue, D., Gutmann, G., Nitta, T., Kabir, A.M.R., Konagaya, A., Tokuraku, K., Sada, K., Hess, H., Kakugo, A., 2019. ACS Nano 13, 12452–12460.
Ishigure, Y., Nitta, T., 2014. Langmuir 30, 12089–12096.
Ishigure, Y., Nitta, T., 2015. IEEE Trans. Nanobiosci. 14, 641–648.
Katira, P., Hess, H., 2010. Nano Lett. 10, 567–572.
Korten, T., Månsson, A., Diez, S., 2010. Curr. Opin. Biotechnol. 21, 477–488.
Lam, A.T.C., Tsitkov, S., Zhang, Y., Hess, H., 2018. Nano Lett. 18, 1530–1534.
Lard, M., ten Siethoff, L., Kumar, S., Persson, M., te Kronnie, G., Linke, H., Månsson, A., 2013. Biosens. Bioelectron. 48, 145–152.
Lin, C.T., Kao, M.T., Kurabayashi, K., Meyhofer, E., 2008. Nano Lett. 8, 1041–1046.
Lodish, H., Berk, A., Kaiser, C.A., Krieger, M., Bretscher, A., Ploegh, H., Amon, A., Martin, K.C., 2016. Molecular Cell Biology, eighth ed. macmillan learning.
Månsson, A., 2012. J. Muscle Res. Cell Motil. 33, 219–233.
Nicolau, D.V., Solana, G., Kekic, M., Fulga, F., Mahanivong, C., Wright, J., Dos Remedios, C.G., 2007. Langmuir 23, 10846–10854.
Nishizaka, T., Miyata, H., Yoshikawa, H., Ishiwata, S., Kinosita, K., 1995. Nature 377, 251–254.
Nitta, T., Hess, H., 2013. Cell. Mol. Bioeng. 6, 109–115.
Nitta, T., Tanahashi, A., Obara, Y., Hirano, M., Razumova, M., Regnier, M., Hess, H., 2008. Nano Lett. 8, 2305–2309.
Rahman, M.A., Salhotra, A., Månsson, A., 2018. J. Muscle Res. Cell Motil. 39, 175–187.
Reuther, C., Catalano, R., Salhotra, A., Vemula, V., Korten, T., Diez, S., Månsson, A., 2021. New J. Phys. 23, 075007.
Romet-Lemonne, G., VanDuijn, M., Dogterom, M., 2005. Nano Lett. 5, 2350–2354.
Saper, G., Hess, H., 2020. Chem. Rev. 120, 288–309.
Scharrel, L., Ma, R., Schneider, R., Jülicher, F., Diez, S., 2014. Biophys. J. 107, 365–372.
Sheehan, P.E., Whitman, L.J., 2005. Nano Lett. 5, 803–807.
Soleymani, L., Li, F., 2017. ACS Sens. 2, 458–467.
Sunagawa, T., Tanahashi, A., Downs, M.E., Hess, H., Nitta, T., 2013. Lab Chip 13, 2827.
Vale, R.D., Milligan, R.A., 2000. Science 288, 88–95.
Walcott, S., Warshaw, D.M., Debold, E.P., 2012. Biophys. J. 103, 501–510.
Winkelmann, D.A., Bourdieu, L., Ott, A., Kinose, F., Libchaber, A., 1995. Biophys. J. 68, 2444–2453.
Yu, T., Wang, Q., Johnson, D.S., Wang, M.D., Ober, C.K., 2005. Adv. Funct. Mater. 15, 1303–1309.